Persistent pressure gradient as a driver of the substorm current wedge: A statistical study

Xiangning Chu[1], Robert McPherron[2], Jacob Bortnik[3], Vassilis Angelopoulos[2], Tung-Shin Hsu[2], James M. Weygand[2], Jinxing Li[3], Xin Cao[1], Homayon Aryan[3]

[1] Laboratory for Atmospheric and Space Physics, University of Colorado Boulder, Boulder, CO, USA

[2] Department of Earth, Planetary and Space Sciences and Institute of Geophysics and Planetary Physics, University of California Los Angeles, California, USA

[3] Department of Atmospheric and Oceanic Sciences, University of California, Los Angeles, California, USA

Corresponding author: Xiangning Chu (chuxiangning@gmail.com)

Key Points:

- Substorm-onset-associated fast flows are located inside the substorm current wedge between two field-aligned currents
- The pressure gradient is well organized by the central meridian of the substorm current wedge
- The substorm current wedge is likely sustained by substorm-scale (>30 min) pressure gradient rather than flow-scale (3 min) flow vortices

Keywords:

- Substorm, substorm current wedge, pressure gradient, flow vortex, field-aligned current

Abstract

The substorm current wedge (SCW) is believed to be driven by pressure gradients and vortices associated with fast flows. Therefore, it is expected that relevant observations are organized by the SCW's central meridian, which cannot be determined using in-situ observations. This study takes advantage of the SCW inversion technique, which provides essential information about an SCW (e.g., location and strengths of field-aligned currents (FACs) and investigates the generation mechanisms of the SCW. First, we have found good temporal and spatial correlations between earthward flows and substorm onsets identified using the midlatitude positive bay (MPB) index. Over half of the flows are observed within 10 minutes of substorm onsets. Most flows (85%) were located inside the SCW between its upward and downward FACs. Second, superposed epoch analysis (SPEA) shows that the onset-associated flow velocity has a flow-scale (3-min) peak, while the equatorial thermal pressure has a substorm-scale (>30 min) enhancement and a trend similar to the westward electrojet and FACs in the SCW. Third, the pressure gradient calculated using in-situ observations is

well organized in the SCW frame and points toward the SCW's central meridian. These facts suggest that the SCW is likely sustained by substorm-scale pressure gradient rather than flow-scale flow vortices. The nonalignment between the pressure gradient and flux tube volume could generate an SCW with a quadrupole FAC pattern, similar to that seen in global MHD and RCM-E simulations. Their magnetic effects on the ground and geosynchronous orbit resemble a classic one-loop SCW.

Plain Language Summary

Substorm current wedge (SCW) formation is believed to be related to the flow braking and diversion process of magnetospheric fast flows. Therefore, the pressure gradients and flow vortices are expected to be organized relative to the center of the current wedge. Obtaining the pattern of pressure gradients and flow vortices requires the knowledge of field-aligned currents (FAC) locations since the current wedge can occur at any local time in the night sector. However, the FAC locations are not available from satellite measurements. In this study, we take advantage of an SCW inversion technique that provides essential information using ground-based magnetic field observations.

First, we found good temporal and spatial correlations between earthward flows during five THEMIS tail seasons and substorm onsets identified using the midlatitude positive bay index. Flow occurrence is found to peak at substorm onset. More than half the flows observed within one hour of substorm onsets occur within ten minutes of onsets. In addition, most of these flows (85%) are found inside an SCW between its upward and downward FACs. It has been suggested that these FACs are generated either by flow vortices, pressure gradients, or both. It is shown here that the flow speed (related to the flow vortices) decays quickly within several minutes. On the other hand, the equatorial thermal pressure (related to the pressure gradient) increases and persists for about an hour and has a trend similar to that for the westward electrojet and FACs of the SCW. Therefore, the SCW is likely sustained by the pressure gradient rather than short-lived flow vortices. The pressure gradient, calculated when three THEMIS probes were distributed in a triangular configuration in the equatorial plane, was found to be well organized relative to the central meridian (CM) of the SCW. The component ∇P_x increases for all substorms; while ∇P_y increases in magnitude and points toward the center of the current wedge. Although the flux tube volume gradient ∇V cannot be obtained from observations, it can be inferred from the magnetic field B_Z allowing for a determination of the sense of the FACs. The peak of increased B_Z was more tailward than the peak of the thermal pressure increase. The nonalignment of ∇P and ∇V should generate an SCW with a quadrupole FAC pattern, similar to that seen in global MHD and RCM-E simulations. In these simulations, the inner current loop is weaker than the outer loop so that the magnetic effect at geosynchronous orbit and on the ground is that of the outer loop diminished in strength by the inner loop, which resembles a classic SCW.

1. Introduction

A substorm current wedge (SCW) is an essential current system associated with magnetospheric substorms. It consists of a reduction of the cross-tail current in the magnetotail, a pair of field-aligned currents (FACs) connecting the cross-tail current with the ionosphere (one flowing into, and the other flowing out of the ionosphere), and a westward electrojet flowing in the ionosphere that connects two FACs. An SCW is believed to be generated by flow braking in the near-Earth region [*Haerendel*, 1992; *Shiokawa et al.*, 1997; *Shiokawa et al.*, 1998a; *Shiokawa et al.*, 1998b; *Kepko et al.*, 2012]. Note that although substorms are triggered by reconnection-generated earthward flows [*Hones et al.*, 1973; *Hones*, 1977; Angelopoulos et al., 2008], the flows can occur at any level of magnetic activity [*Angelopoulos et al.*, 1994]. The fast flows are more common than substorms, and there is no one-to-one correspondence between them [*McPherron et al.*, 2011]. Furthermore, the speed of earthward flow drops significantly inside 12 R_E [*McPherron et al.*, 2011], which is the flow braking region where SCWs are generated. It was suggested that the magnetic flux accumulation in the inner magnetosphere is correlated with the strength of a substorm current wedge [*Chu et al.*, 2021]. Therefore, it is reasonable to expect earthward flows in the flow braking region to correlate better with SCW formation than fast flows in the middle magnetotail. However, which mechanisms and parameters determine whether a fast flow can trigger a global substorm versus a pseudo breakup is still unknown. The temporal and spatial correlation of fast flows with the substorm current wedge, which is essential to study the SCW mechanisms, is investigated in this paper.

Substorm current wedge formation has been studied using theory, simulations, and observations [*Birn et al.*, 1999; *Keiling et al.*, 2009; *Xing et al.*, 2010; *Yao et al.*, 2012; *Birn and Hesse*, 2014; *Kepko et al.*, 2015]. Theory suggests that the FACs in an SCW are generated by an inertial current, flow vortices, and pressure gradients [*Vasyliunas*, 1970]. The inertial current is usually neglected because it is considerably weaker than the current created by flow vortices and pressure gradients [*Haerendel*, 1992; *Shiokawa et al.*, 1997; *Shiokawa et al.*, 1998a; *Shiokawa et al.*, 1998b; *Birn et al.*, 1999]. On the other hand, event studies show that flow vortices and pressure gradients can generate strong FACs to support a typical SCW [*Keiling et al.*, 2009; *Xing et al.*, 2010; *Yao et al.*, 2012]. Global MHD simulations suggest that a depleted plasma bubble with thermal pressure lower than the ambient plasma flowing earthward can set up flow vortices and azimuthal pressure gradient pointing away from the flow, generating a quadrupole distribution of FACs [*Birn and Hesse*, 1991; 2014]. A quadrupole SCW has an outer current loop the same as pictured in the classic SCW (usually referred to as a region-1-sense current) and a weaker inner current loop flowing in the opposite direction at the same local time (referred to as a region-2-sense current). The magnetic effect of the inner current loop partially cancels the effect of the outer loop on the ground and in geosynchronous orbit. Thus, their combined magnetic effect is equivalent to a classic SCW with current corresponding to the difference current. Therefore, as suggested by simulations, the pressure gradients and flow vortices are expected to be organized relative to the

central meridian of the current wedge. Obtaining the pattern of pressure gradients and flow vortices requires the knowledge of FAC locations since the current wedge can occur at any local time in the night sector. The FAC locations cannot be determined from in-situ observations because FACs are weak and spread over large regions relative to the satellite coverage. Furthermore, in-situ observations are sometimes transient and localized and not necessarily related to a global SCW. In addition, the generation mechanisms of the FACs, including the pressure gradient and flow vortices, are supposed to be well organized by the central meridian of the SCW (i.e., in the SCW frame). This paper will examine the pattern of the pressure gradients and flow vortices in the SCW frame. The central meridian of the SCW will be obtained using the FACs locations obtained from the SCW inversion technique using ground magnetometer data based on the positive bay signature at midlatitudes [*Chu et al.*, 2014].

The database of the flows and substorm onset is described in section 2. Then, the observations and statistical analysis are presented in section 3. Finally, we discuss the implication of the analysis in section 4.

1. Data and model

The auroral electrojet indices (AE and AL) at a 1-min resolution from the World Data Center for Geomagnetism are used to indicate the strength of the westward electrojet in the SCW. The midlatitude positive bay (MPB) index, designed to indicate the strength of the FACs in the SCW, is calculated at a 1-min resolution using magnetometer data at midlatitudes from InterMagnet [*Chu et al.*, 2015]. A substorm onset list is first identified using the MPB index and then refined using original magnetometer data [*Chu et al.*, 2015]. The timing of maximum substorm development is identified when the MPB index reaches its maximum. The end of the substorm is identified when the MPB index decreases to a quiet level. Note that the MPB index was designed to detect major onsets, and it is less sensitive to pseudo breakups and localized intensifications (see details in [*Chu et al.,* 2015; McPherron and Chu, 2016a, b; McPherron and Chu, 2018]). Furthermore, the strength and location of the SCW are obtained every minute using the SCW inversion technique [*Chu et al.*, 2014]. The inversion technique takes ground magnetometer data at midlatitudes as input and determines the optimal parameters of the current system, including the location and strength of the FACs in the SCW.

The observations in the magnetotail are obtained from the identically-instrumented Time History of Events and Macroscale Interactions during Substorms (THEMIS) probes (P1-P5) during five tail seasons from 2008 to 2012 [*Angelopoulos*, 2008]. The apogees of the five probes are 30 R_E for P1, 20 R_E for P2, and 10-12 R_E for P3, P4, and P5. The fluxgate magnetometer (FGM) provides three-second spin-averaged magnetic field [*Auster et al.*, 2008]. The electrostatic analyzer (ESA) obtains ion and electron measurements in the 5 eV to 25 eV energy range [*McFadden et al.*, 2008]. The solid state telescope (SST) obtains ion and electron fluxes in the 25 keV to 1 MeV range (Angelopoulos, 2008). The joint plasma moments (density, velocity, and tem-

perature) have been calculated from a combination of the measurements from both ESA and SST instruments with proper calibrations (e.g., subtraction of the effect of spacecraft potential, sun-contamination, and detector calibration) [*Angelopoulos*, 2008].

A list of earthward flows is created using THEMIS observations from P3, P4, and P5 in the nightside near-Earth magnetotail region using the following criteria, which are adopted in many previous studies (e.g., McPherron et al., [2012]; Kissinger et al., [2012]). The nightside observations are confined to a cylindrical region bounded by $\sqrt{Y^2 + Z^2} < 12R_E$, X<0 R_E and $\sqrt{X^2 + Y^2 + Z^2} > 6R_E$. Observations are restricted to the plasma sheet by requiring plasma beta ( ), the ratio of thermal pressure to magnetic pressure, to be greater than 0.5. The plasma velocities are converted to parallel ($V_\parallel$) and perpendicular velocities ($V_\perp$) relative to the background magnetic field. Fast earthward flows are defined as $V_x \geq 0$ km/s and $V_{xy} \geq 150$ km/s, where V_{xy} is the flow velocity in the GSM coordinates. Flow onsets are defined when V_{xy} exceeds 100 km/s, and the end is defined when V_{xy} is lower than 100 km/s. In addition, another list of earthward flows in the mid magnetotail is created using THEMIS P2, whose apogee is about 20 R_E, during the first two tail seasons in 2008 and 2009. Unless otherwise specified, the earthward flows are those observed by THEMIS P3, P4, and P5 earthward of 12 R_E.

1. Observations

   (a) Substorm event analysis

Figure 1 shows an overview of an isolated substorm between 01:20 UT and 02:00 UT on February 07, 2008. The MPB and AL indices in the first two panels indicate the strengths of the FACs and the westward electrojet of the SCW, respectively. They started to change sharply at ~01:28 UT, which is identified as the substorm onset. The MPB index reached its maximum at 01:43 UT, and the AL index was close to its maximum value during the same period. The two indices showed that the SCW lasted for ~30 minutes. The locations of the upward and downward FACs in the SCW, obtained from the SCW inversion technique [Chu et al., 2014], are shown in magnetic local time (MLT). The downward FAC was located at 03:00 MLT, and the upward FAC at around 19:00 MLT. The central meridian of the SCW was located at 23:00 MLT.

As shown by the thin, nearly horizontal lines, THEMIS satellites were located at 23:00 MLT at the onset. They were co-located with the SCW central meridian at the onset and shifted duskward of it after the onset. Three THEMIS satellites observed earthward flows of ~1000 km/s in the central plasma sheet (beta >1) at the onset, which lasted for roughly 2 minutes. Thus, the earthward flows were observed at the SCW central meridian and inside the SCW between the two FACs. No other earthward flow was observed during the remainder of the substorm. The equatorial thermal pressure was calculated using $P_{eq} =$

$P_{\mathrm{th}} + \frac{(B_x^2+B_y^2)}{2\mu_0}$, assuming that $\mathrm{B_Z}$ was relatively constant near the current sheet [*Xing et al.*, 2009; *Xing et al.*, 2011].

The pressure gradient ∇P has been calculated under a linear variation assumption since three THEMIS probes were very close (within 2 $\mathrm{R_E}$) and in a triangular configuration on the equatorial plane (bottom panel). First, the equatorial thermal pressure ($\mathrm{P_{eq}}$) started to increase after the earthward flow and sustained for 30 minutes throughout the substorm, much longer than the flow duration. Second, the variation in the pressure $\mathrm{P_{eq}}$ and pressure gradient ∇P showed two distinct patterns: flow-scale (3 min) and substorm-scale (30 min). When the earthward flows were observed at substorm onset, the equatorial pressure $\mathrm{P_{eq}}$ started to increase and was associated with strong fluctuations. The pressure gradient ∇P_x increased from a background of 0.7 nPa/R_E to 1.4 nPa/R_E while the azimuthal ∇P_y turned from roughly zero to a negative peak of $\nabla P_y = -4\ nPa/R_E$. It suggests that the thermal pressure was higher earthward and eastward. When the flows disappeared after 3 min, the pressure gradient ∇P dropped quickly to the background value. On the other hand, a substorm-scale pressure enhancement developed during the substorm expansion phase. The radial pressure gradient ∇P_x persisted in being positive and increased slightly (1.2 nPa/R_E). The azimuthal pressure gradient reached $\nabla P_y = -1.5\ nPa/R_E$, which was weaker than the peak value during flows but lasted longer. It suggests that a substorm-scale pressure gradient persisted earthward and toward the SCW's central meridian. Most importantly, the timescale and trend of the pressure gradient were similar to that of the westward electrojet and FACs in the SCW, as indicated by the AL and MPB indices.

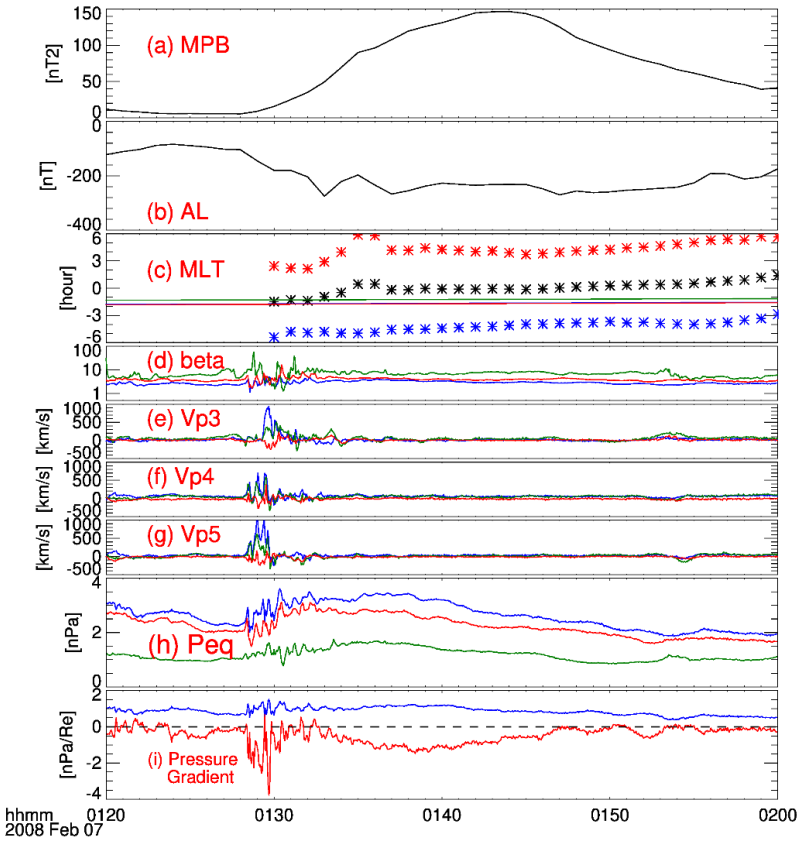

Figure 1. An overview of observations for an isolated substorm on February 07, 2008. The panels show: (ab) MPB and AL indices; (c) the MLT locations of the upward (blue) and downward (red) FACs and their central meridian (black) are shown in asterisks. The MLT of THEMIS P3 (blue), P4 (green), and P5 (red) are shown as solid lines. The plasma beta at the location of the THEMIS probes is shown in the fourth panel. The flow velocity in GSM coordinates at THEMIS probes is shown in the following three panels (blue, green, and red for the x, y, and z directions). The equatorial thermal pressures observed at the three THEMIS satellites are shown in the next panel for P3(blue), P4 (green), and P5 (red). The pressure gradients ∇P_x (blue) and ∇P_y (red) are shown in the last panel.

1. Temporal correlation between flows and substorm onsets

The substorm onset is believed to be triggered by the reconnection-generated earthward fast flows [Angelopoulos et al., 2008; Pu et al., 2009; Chu et al., 2009]. Therefore, the fast flows are usually observed within a few minutes of the substorm onset. This study investigates the temporal correlation between

the earthward flows and substorm onsets.

Figure 2a shows the time delay analysis between earthward flows observed within 12 R_E and substorm onsets within a time window of $\pm$ 1 hour. The MPB substorm onset was set to epoch zero in the time delay analysis. Thus, a positive (negative) time delay means that flows were observed after (before) the substorm onset. A total of 703 flows were observed within 1 hour of substorm onset, using the selection criteria described in Section 2. A sharp peak was found at epoch zero in the time delay distribution. More than half of these flows (356) were found within 10 minutes of substorm onsets, referred to as onset-associated flows. The close temporal correlation suggests that most flows were observed simultaneously with substorm onsets.

The flow occurrence during different substorm phases is investigated in Figure 2b. Because the substorm durations vary between events, they were normalized to 1 and divided into ten bins. The substorm duration is defined as the interval between the substorm onset and the end of the substorm [*Chu et al.*, 2015]. The mean value of the substorm duration is 46 minutes. A total of 1299 flows were found in the interval between -1 to 2 substorm durations. The flow occurrence normalized by substorm duration was also seen to be peaked at substorm onset. The flow occurrence was much lower at other substorm phases, but not zero. Furthermore, the flow occurrence during the substorm growth phase before the substorm onset was slightly higher than after the substorm onset.

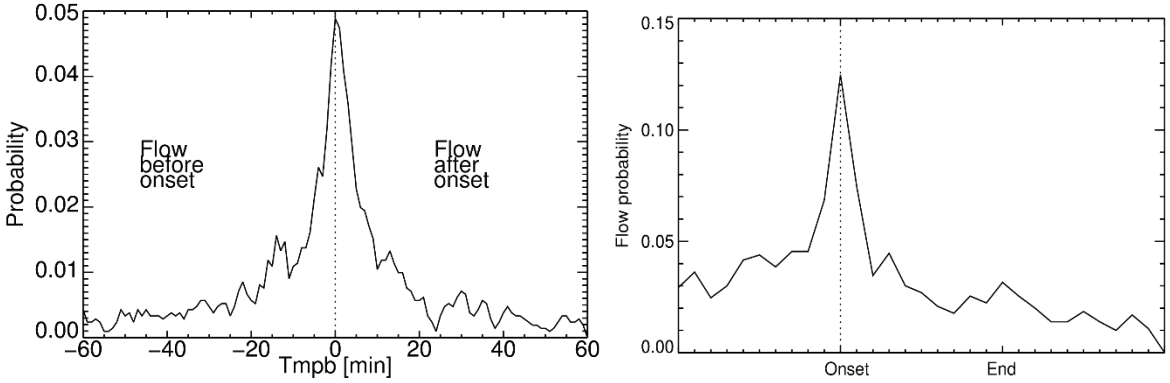

Figure 2. (a) Time delay analysis between the earthward flows observed by THEMIS P3, P4, and P5 within 12 R_E and substorm onsets identified using the MPB index. The substorm onsets have been set to epoch zero. The positive (negative) delay means that flows were observed after (before) the substorm onsets. (b) The probability of flows is normalized by substorm duration.

1. Spatial correlation between flows and SCWs

Figure 1 shows that the MLT locations of the onset-associated earthward flows were inside the SCW and positioned between the MLT locations of the two FACs. Statistical analysis was carried out to study the spatial correlation between the

earthward flows and the FACs. Only onset-associated flows were selected to ensure the locations of the FACs were available (see the second paragraph in section 3.2 for details). Then, the locations of the FACs were determined using the SCW inversion technique [Chu et al., 2014]. Since the SCWs have different MLT widths for different substorms, the SCW widths are normalized to one where the location of the upward FAC is set to zero, and the downward FAC is set to one. Figure 3 shows the probability of the flows' locations relative to the FACs. The probability peaks inside the SCW between two FACs. Among the 589 flows associated with substorm onset, more than 85% (501) were found inside an SCW. Moreover, the occurrence distribution was asymmetric and skewed toward the duskside (upward) FAC. An SCW is also asymmetric because the two FACs have different widths. The upward FAC is usually narrow, and the downward FAC is wider, as illustrated by the horizontal bars at the top of Figure 3 [*Chu et al.*, 2014]. The spatial correlation between the onset-associated flows and the FACs is consistent with the view that the earthward flows generate upward FAC on their duskside and downward FAC on their dawnside.

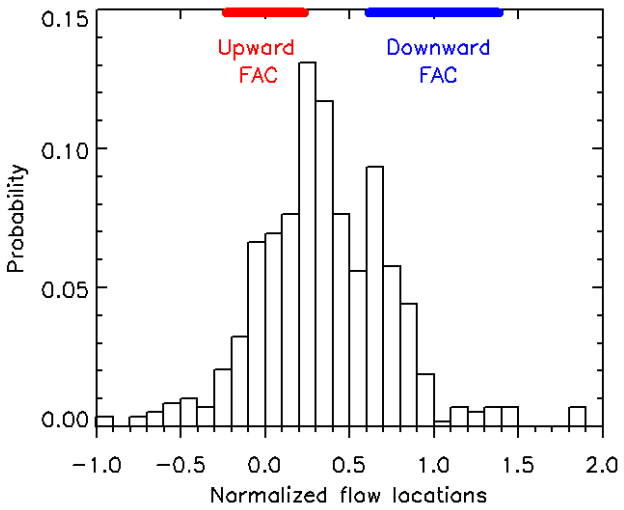

Figure 3. The probability distribution of spacecraft-observed flow locations associated with substorm onset as a function of the FAC locations in the SCW, inverted from the ground magnetometers. The FACs' locations have been normalized so that the location of the upward (downward) FAC is located at zero (one). The FAC widths are indicated by horizontal bars at the top. More than 85% of the flows are between the upward and the downward FACs.

1. Pressure and flows

Superposed epoch analysis (SPEA) of the flow velocity and the equatorial thermal pressure was used to investigate the potential contribution of flow vortices

and pressure gradients to the FAC generation. Figure 4 shows the SPEA of the MPB and AL indices, equatorial thermal pressure, magnetic field B_Z, and flow velocity. The epoch zero is set to the onset-associated flows. Both the MPB and AL indices started to change sharply at epoch zero, suggesting that the FACs and the westward electrojet in the SCW strengthened. These currents reached a maximum within about 20 minutes and then gradually decayed within about an hour. The equatorial thermal pressure increased sharply at epoch zero and slowly decayed within about an hour. The magnetic field B_Z rapidly increased after the onset, reaching a maximum in ~20 minutes, and then slowly decreased, indicating a magnetic dipolarization and consequent reduction in the cross-tail current associated with the SCW formation. The trends of the equatorial thermal pressure and the magnetic dipolarization are similar to those of the currents in the SCW. On the other hand, the flow velocity had a sharp peak at epoch zero and quickly decayed within a few minutes. Although the flow occurrence was non-zero after the onset in Figure 2, the SPEA of the flow velocity was smeared out by quiet periods without flows. It should be noted that the equatorial thermal pressure reached its maximum much quicker than the dipolarization of B_Z. In other words, the peak center of B_Z arrived later than the peak center of the equatorial thermal pressure. It suggests that the center of B_Z was more tailward than the center of the pressure increase.

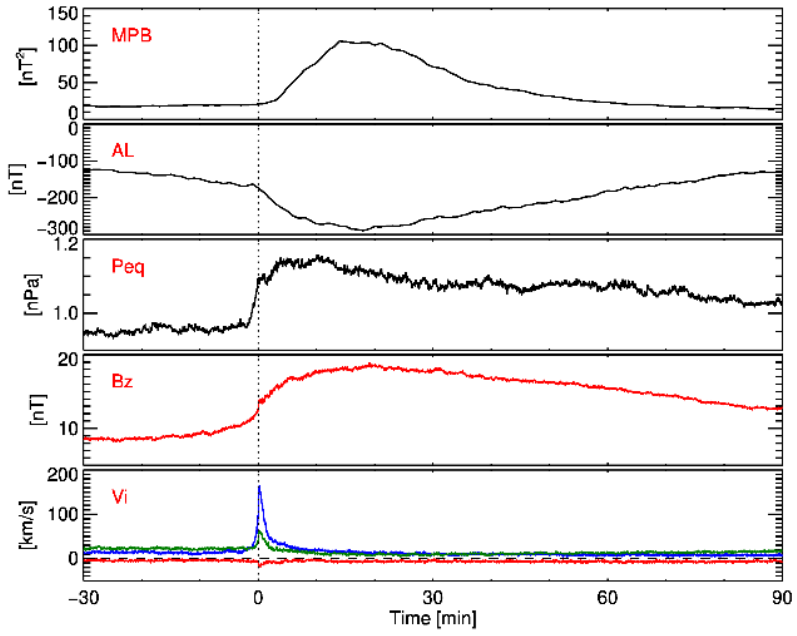

Figure 4. Superposed epoch analysis of the MPB and AL indices, the equatorial thermal pressure, the magnetic field B_Z, and the flow velocity relative to the onset-associated flows within 12 R_E.

Figure 5 shows the SPEA of the equatorial thermal pressure, plasma thermal pressure, plasma density, temperature, and magnetic field B_Z relative to flows in the mid-tail observed by THEMIS P2 (from -12 to -20 R_E). Note that the equatorial thermal pressure was almost constant after detecting the flows. Although the plasma density decreased in the plasma bubble, the plasma temperature increased significantly. Therefore, the thermal pressure increased after the flow onset. The magnetic field B_Z had a short spike of 2 min at the flow onset, which was associated with the dipolarization front ahead of the fast flow (e.g., [*Runov et al.*, 2009; *Liu et al.*, 2014] and references therein). The B_Z reached its maximum value in about 10 minutes and slowly decreased. The percentage change in B_Z was larger than the change in the equatorial thermal pressure. Therefore, in the mid-tail region (-12 to -20 R_E), the magnetic dipolarization was observed while the equatorial thermal pressure remained almost constant.

The results above suggest that as fast flows travel earthward, plasma temperature and equatorial thermal pressure increase, with most of the heating occurring in the near-Earth region (within -12 R_E). On the other hand, the elevated flow velocity did not last long enough to sustain an SCW, which endured for much longer. Therefore, the pressure gradient resulting from the substorm-scale increased pressure is more likely to be the sustaining mechanism of the FACs of the SCW. This fact is consistent with our previous study showing that the SCW strength correlated with the substorm-scale magnetic flux accumulation in the inner magnetosphere [*Chu et al.*, 2021].

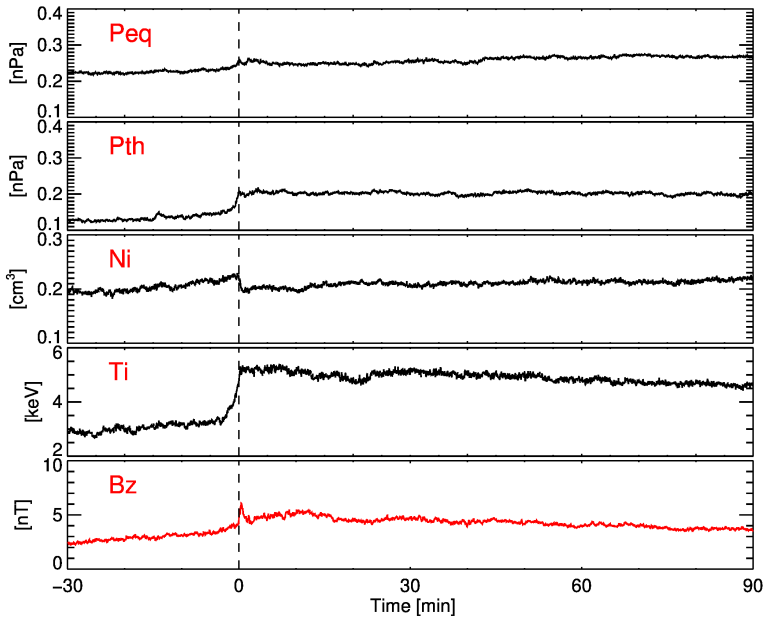

Figure 5. Superposed epoch analysis of the equatorial thermal pressure, plasma

thermal pressure, plasma density, thermal temperature, and the magnetic field B_Z relative to the flows observed in the mid-tail region, defined to be between -12 and -20 R_E.

1. Pressure gradient in SCW frame

This section investigates the pressure gradient distribution in the SCW frame. Three THEMIS probes (P3, P4, and P5) must be located in a triangular configuration near the equatorial plane and close to each other (within 2 R_E) to calculate the pressure gradient. During five tail seasons, 42 time intervals with a total of 253 hours of data satisfy these criteria. A large fraction of intervals occurred in 2008 because the THEMIS probes were separated in the z-direction in later years. Twenty-three isolated substorms, including the substorm example in Figure 1, were found in these time intervals. The FAC locations and central meridian of the SCW were obtained for each event using the SCW inversion technique. The change in the equatorial thermal pressure was obtained by subtracting the initial value at the onset. Then, the pressure gradient ∇P was calculated using data from three THEMIS satellites. Figure 6 shows the changes in ∇P_x and ∇P_y as a function of local time relative to the central meridian of the SCW. The ∇P_x , pointing toward the Earth, increased during most of the substorms, suggesting that the equatorial pressure increased with decreasing distance, in moving closer to the Earth. The ∇P_y, pointing duskward, increased on the dawnside of the central meridian, and decreased on the duskside, suggesting that the maximum equatorial thermal pressure was co-located with the central meridian of the SCW. This fact is consistent with the results shown in Figure 3 that the flows were located inside the SCW between two FACs, supporting the idea that the high-pressure region created in the flow braking process was co-located with the central meridian of the SCW. As a result, the downward FAC was generated on its dawnside and the upward FAC on its duskside.

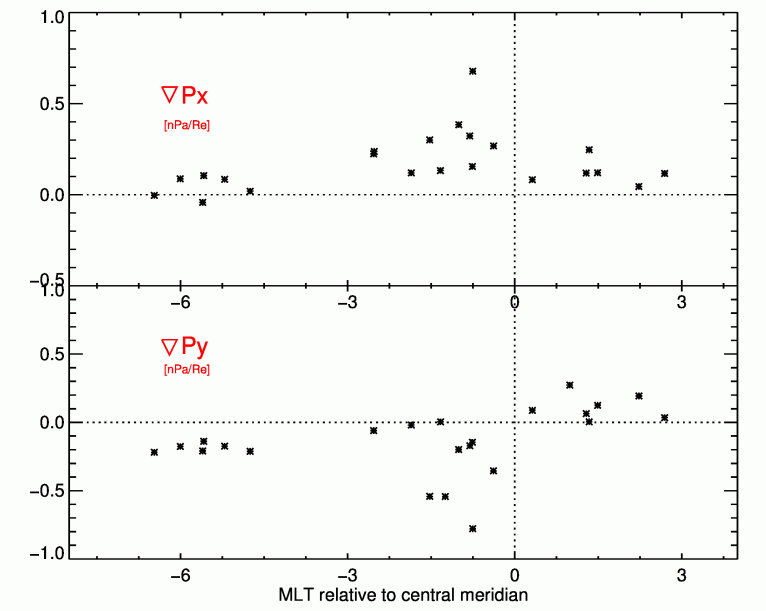

Figure 6. The changes in the components of the pressure gradients ∇P_x and ∇P_y during substorms as a function of local time relative to the central meridian of the SCW.

1. Discussion

Substorm current wedge formation is usually attributed to pressure gradients and flow vortices generated in the flow braking and diversion process [*Vasyliunas*, 1970; Yao et al., 2012; Kepko et al., 2015 and references therein]. The pressure gradients and flow vortices are expected to be organized relative to the central meridian of the SCW, i.e., in the SCW frame. Unfortunately, the central meridian of the SCW could not be readily obtained from in-situ satellite observations in past studies. In this study, we obtained the central median of the SCW using the SCW inversion technique based on ground magnetometer data. Then, we statistically investigated the generation mechanisms of the FACs in the SCW frame. In this section, we discuss how these results may shed light on the generation mechanisms of the SCW.

1. Flow occurrence relative to substorm onset

Although earthward flows are associated with substorms, they can nevertheless occur at any level of magnetic activity [*Angelopoulos et al.*, 1994], and there is no one-to-one correspondence between them [*McPherron et al.*, 2011]. Since the SCW is believed to be generated in the flow braking region inside 12 R_E, we investigated the temporal and spatial correlation between the earthward flows inside 12 R_E and substorms identified using the MPB index. Figure 2a shows the time delay analysis between the flows and substorms with a one-hour time window. The flow occurrence peaks at substorm onset, and more than half of the

flows were observed within 10 min of substorm onset. A similar close temporal correlation was found between earthward flows and substorm onsets identified using the AL index [*McPherron et al.*, 2011]. The flow occurrence normalized by the substorm duration in Figure 2b also peaks at substorm onset. These results support the idea that SCW formation is associated with flow braking within 1-2 minutes. It should be noted that the flow occurrence is non-zero all the time, consistent with the fact that flows can occur at any level of magnetic activity and with recent studies showing that only a small fraction of fast flows can trigger a substorm [*Ohtani et al.*, 2006; *Takada et al.*, 2006; *Weygand et al.*, 2008]. The penetration depth of an earthward flow is generally thought to depend on its entropy, rather than its initial flow velocity [*Dubyagin et al.*, 2010; 2011; *Sergeev et al.*, 2014a]. The flow has an entropy lower than the ambient plasma when generated by magnetic reconnection [*Pontius and Wolf*, 1990]. The flow is expected to move earthward adiabatically, conserving its lower entropy, and reaches a location where the background plasma entropy equals that of the flow. It should also be noted that the flow occurrence is higher before the substorm onset during the growth phase and lower during the expansion phase. The occurrence of ground Pi 2 pulsations, associated with fast flows, was also shown to be higher during the substorm growth phase [*McPherron*, 1994]. It is possible that the magnetic energy stored in the tail lobe is released by the onset-associated reconnection so that another magnetic reconnection does not occur until enough energy is again stored in the tail lobe. It is also possible that the magnetic field lines in the inner magnetosphere become highly dipolarized during the expansion phase, which makes it more difficult for flows to penetrate the near-Earth region. In other words, the background entropy decreases when the magnetic field lines become dipolarized, and thus the flows stop at locations further from the Earth.

1. Flow locations in the SCW frame

The statistical results shown in Figures 2 and 3 indicate a close temporal and spatial correlation between the flows and the SCW. According to numerical simulations, the pressure gradient and the FACs are expected to be organized by the MLT location of the flows. Although the occurrence distribution of the flows is centered at 23:00 MLT, the flows can reach the nightside inner magnetosphere from any local time [*McPherron et al.*, 2011]. In addition, the central meridian of the SCW is also centered at 23:00 MLT, but it can be anywhere in the nightside. In this study, the spatial correlation between the flows and the SCWs has been investigated statistically for the first time. As shown in Figure 3, more than 85% of the onset-associated flows were located inside the SCW between the MLT locations of the two bounding FACs, suggesting that FACs are usually located on both sides of the flow. In other words, these results support the mechanism that earthward flows generate FACs of different polarities on each side, and are further consistent with numerical simulations of the current wedge formation, in which the pressure gradients and the flow vortices have different polarities on each side of the flows, generating FACs of different polarity.

In addition, the flow distribution shown in Figure 3 is asymmetric, skewed toward the duskside of the flow. The FACs in an SCW are also asymmetric due to their different current carriers, with narrow upward FACs and wider downward FACs. The skewness of the flow distribution in the SCW frame is likely due to the asymmetry of the FACs. One possible reason is that ion acceleration is more effective on the duskside of the flows, and the plasma is heated more on the duskside [*Zhou et al.*, 2014a; *Zhou et al.*, 2014b]. The asymmetry in plasma heating might produce an asymmetric pressure increase; thus, asymmetric pressure gradients generate asymmetric FACs. The asymmetric pressure distribution is also evident in Figure 6, in which both ∇P_x and ∇P_y are stronger on the duskside in the SCW frame, resulting in FACs with stronger current density on the duskside.

1. Substorm current wedge generation mechanisms

In this study, we investigated the contributions of the pressure gradients and flow vortices to the generation of the SCW's FACs. As shown in Figure 4, the FACs and westward electrojet in the SCW increased sharply after the onset and lasted for about an hour. The equatorial thermal pressure also increased after the onset and had a temporal trend similar to the strength of the SCW. However, the earthward flows lasted for less than 3 minutes, significantly shorter than the SCW measured by the MPB and AL indices on the order of ~30 minutes. Therefore, the pressure gradient is likely to be the sustaining mechanism responsible for the FACs in the SCW rather than the flow vortices. An event study showed that a flow vortex with a peak speed of 500 km/s and a radius of 1 R_E could generate enough FACs for an SCW [*Keiling et al.*, 2009]. Another event study found that the total FACs from the flow vortices and the azimuthal pressure gradient are comparable to a typical SCW [*Yao et al.*, 2012]. The flow vortices lasted less than 5 minutes in both studies. Therefore, although flow vortices and azimuthal pressure gradients could generate FACs having a strong current density initially, the pressure gradient is likely the dominant contributor to the FACs in an SCW because the flow vortices disappear quickly. To further validate this conclusion, it is necessary to have multiple in-situ measurements to confirm the existence of the flow vortices and examine their contribution to the FACs, which requires a satellite constellation such as the proposed Magnetospheric Constellation mission (MagCON) [*Kepko et al.*, 2018].

The equatorial thermal pressure observed within 12 R_E showed a substorm-scale (~1 hour) increase of ~20%, as shown in Figure 4. In contrast, in the mid-tail (from -12 to 20 R_E), the equatorial thermal pressure showed only a flow-scale transient change (~2 min). In addition, the equatorial thermal pressure in the mid-tail did not decrease within the flow, suggesting a picture slightly different from previous simulations in which the thermal pressure decreased inside the flow [*Yang et al.*, 2011; *Birn and Hesse*, 2013]. This result does not contradict previous statistical studies showing that thermal pressure decreases after a dipolarization front [*Runov et al.*, 2011; *Liu et al.*, 2013b]. In their results, the decrease in the thermal pressure lasted less than two minutes and

then increased above the background level. Furthermore, the transient drop in the pressure corresponds to a localized current structure surrounding the dipolarization front rather than a global SCW. As shown in Figure 1, both flow-scale and substorm-scale pressure gradients are observed in the course of a substorm. The flow-scale pressure gradient was associated with a decrease in the equatorial pressure during the flow interval; the substorm-scale pressure gradient was associated with increased equatorial pressure even when no flow was present. The flow-scale pressure gradient is usually related to a narrow current system (current wedgelet) [*Birn and Hesse*, 2013; *Liu et al.*, 2015] and the substorm-scale pressure gradient to the global SCW.

Because the pressure gradient seems to sustain the global SCW, the pressure gradient pattern was investigated in the SCW frame. Figure 6 demonstrates that ∇P_x increased for almost all substorm events, suggesting that the thermal pressure becomes higher at decreasing distances toward the Earth. The ∇P_y was negative on the duskside of the central meridian and positive on the dawnside, pointing toward the central meridian, and increasing in intensity on either side. Therefore, it can be concluded that the azimuthal pressure gradient is well organized in the SCW frame, suggesting that the equatorial thermal pressure is higher closer to the central meridian of the SCW. In other words, the center of the high pressure created by flow braking is co-located with the central meridian of the SCW. This result is consistent with FAC generations on each side of the flows, as shown in Figure 4. In addition, both ∇P_x and ∇P_y are larger on the duskside than on the dawnside, likely corresponding to stronger current density. The asymmetry in the pressure gradient may be responsible for an asymmetric SCW (with narrower, stronger upward FACs and weaker, wider downward FACs). The results also suggest that the earthward flow heats the ambient plasma as it travels earthward, leaving a high-pressure region behind it. The equatorial pressure increased faster than the magnetic field B_Z in the near-Earth region.

The current density of the FACs is determined not only by pressure gradient ∇P but also by the gradient of flux tube volume ∇V. However, ∇V cannot be accurately obtained from in situ observations since it is determined by an integration along the flux tube from the magnetosphere to the ionosphere. It can, however, be roughly inferred from the magnetic dipolarization. As shown in Figures 4 and 5, the equatorial pressure increased faster than B_Z in the near-Earth region. Thus, the center of B_Z was more tailward than the equatorial thermal pressure. This configuration of the equatorial pressure and B_Z is similar to the RCM-E simulation of an idealized plasma sheet bubble (Figure 5 in [*Yang et al.*, 2011]), in which a quadrupole pattern of FACs is generated.

Figure 7 shows an illustration of the substorm current wedge formation. Magnetic reconnection generates an earthward flow with a dipolarization front (or reconnection front) [*Angelopoulos et al.*, 2013], which accelerates the plasma ahead of it and forms a high-pressure front [*Zhou et al.*, 2014a]. The currents surrounding a dipolarization front are related to narrow current wedgelets in the

ionosphere [*Liu et al.*, 2013a; *Liu et al.*, 2015]. As the flow approaches the near-Earth region, especially the transition region, it quickly slows down and diverts azimuthally [*McPherron et al.*, 2011]. The flow braking and diversion create two flow vortices on each side and a high-pressure region. Initially at the onset, both the flow vortices and the pressure gradient generate FACs that support the SCW [*Keiling et al.*, 2009; *Yao et al.*, 2012]. The flow vortices disappear within several minutes as the flow vanishes. The high pressure lasts for about an hour, and the associated pressure gradient sustains the SCW. The peak of magnetic dipolarization is located more tailward than the high-pressure region, as illustrated in Figure 7. According to the Vasyliunas equation, the nonalignment between their gradients generates an SCW with quadrupole FACs. The outer current loop is a classic SCW, a region-1-sense current loop; the inner current loop is a region-2-sense current loop. The existence of quadrupole SCW was also suggested by previous simulations [*Yang et al.*, 2011; *Birn and Hesse*, 2014] and observations [*Sergeev*, 2013; *Sergeev et al.*, 2014b]. The combined magnetic effects of these FACs on the ground and in geosynchronous orbit can be represented by their net current, similar to a classic SCW.

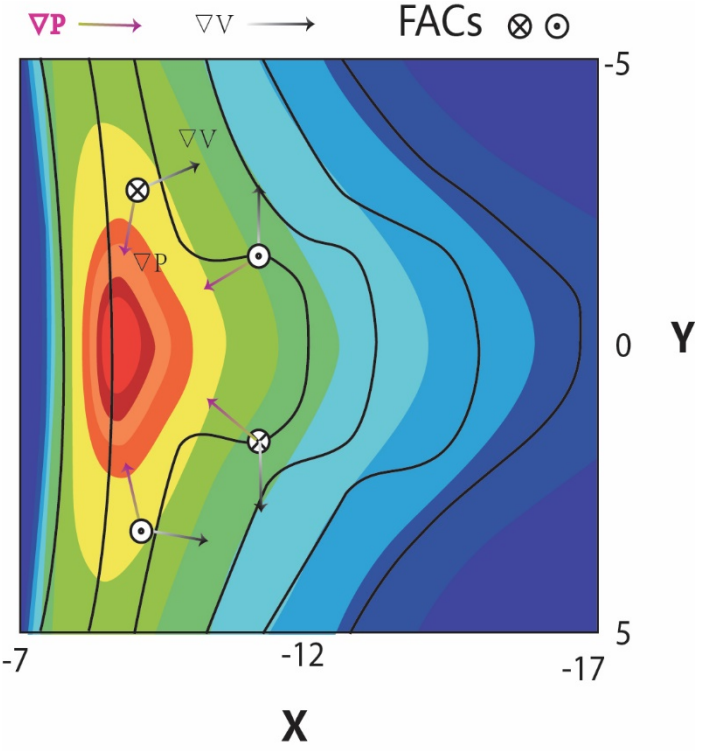

Figure 7. Cartoon illustration of substorm current wedge formation. The color contour shows the plasma pressure on the equator. The lines are the contours of the magnetic field B_Z. The purple and black vectors represent the gradient of thermal pressure and flux tube volume. The directions of the FACs are obtained

from the Vasyliunas equation.

1. Conclusions

This study investigates substorm current wedge (SCW) formation using a set of earthward flows observed during five THEMIS tail seasons and substorm onsets identified using the MPB index. It is found that the flow occurrence has flow-scale (few minutes) peaks at substorm onsets, as shown in the time delay analysis, and the flow speed quickly dropped in 3 minutes. The close temporal correlation between the fast flows and substorm onsets suggests that SCW formation is highly correlated with the flow braking process. In addition, it is found that most (85%) of the onset-associated flows were spatially located inside the MLT region of the SCW, between the two FACs. Such a good spatial correlation supports the mechanism that FACs are generated on both sides of the flows.

The equatorial thermal pressure and flow vortices relative to the flow onsets were investigated, and it was found that the equatorial thermal pressure has a substorm-scale enhancement and lasts for about an hour, comparable to the durations of the FACs and westward electrojet in the SCW. On the other hand, the flows related to the flow vortices lasted for less than 3 minutes, which was significantly shorter than the SCW. The different time scales suggest that the SCW may be generated by pressure gradient and flow vortices in the first few minutes before the flows decayed. However, the SCW is likely sustained by substorm-scale high-pressure generated in the flow braking process rather than flow-scale flow vortices.

Furthermore, the pressure gradient was found to be well organized in the SCW frame. The ∇P_x increased for almost all substorms; the ∇P_y increased on its dawnside of the central meridian and decreased on its duskside. This fact suggests that the center of the high-pressure region caused by flow braking is co-located with the central meridian of the SCW, which is consistent with the theory that FACs are generated on both sides of the flows. Although the gradient of the flux tube volume cannot be obtained from in situ observations, it can be inferred from the magnetic dipolarization of B_Z. The center of the magnetic dipolarization was more tailward than the center of the increased pressure, which is consistent with simulation results. As a result, the nonalignment between the gradient of the flux tube volume and pressure can generate an SCW with quadrupole FACs. Their combined magnetic effects on the ground and geosynchronous orbit are similar to their net current, which resembles a classic one-loop SCW.

1. Acknowledgments

The authors would like to thank NASA HSR award 80NSSC18K1227 for their generous support of this project. X. C. is supported by grants 80NSSC19K0911, 80NSSC20K0196 and 80NSSC20K1325. We gratefully acknowledge THEMIS, INTERMAGNET, SuperMAG, and their data providers.

Data access and processing were done using SPEDAS Angelopoulos et al., 2019().

1. References:

Angelopoulos, V. (2008), The THEMIS Mission, *Space Sci. Rev.*, *141*(1), 5-34, doi:10.1007/s11214-008-9336-1.

Angelopoulos, V., C. F. Kennel, F. V. Coroniti, R. Pellat, M. G. Kivelson, R. J. Walker, C. T. Russell, W. Baumjohann, W. C. Feldman, and J. T. Gosling (1994), Statistical Characteristics of Bursty Bulk Flow Events, *J. Geophys. Res.*, *99*(A11), 21257-21280, doi:10.1029/94ja01263.

Angelopoulos, V., A. Runov, X. Z. Zhou, D. L. Turner, S. A. Kiehas, S. S. Li, and I. Shinohara (2013), Electromagnetic Energy Conversion at Reconnection Fronts, *Science*, *341*(6153), 1478-1482, doi:DOI 10.1126/science.1236992.

Auster, H. U., et al. (2008), The THEMIS Fluxgate Magnetometer, *Space Sci. Rev.*, *141*(1-4), 235-264, doi:10.1007/s11214-008-9365-9.

Birn, J., and M. Hesse (1991), The Substorm Current Wedge and Field-Aligned Currents in MHD Simulations of Magnetotail Reconnection, *J. Geophys. Res.*, *96*(A2), 1611-1618, doi:10.1029/90JA01762.

Birn, J., and M. Hesse (2013), The substorm current wedge in MHD simulations, *J. Geophys. Res.*, *118*(6), 3364-3376, doi:10.1002/jgra.50187.

Birn, J., and M. Hesse (2014), The Substorm Current Wedge: Further Insights from MHD Simulations, *J. Geophys. Res.*, 2014JA019863, doi:10.1002/2014JA019863.

Birn, J., M. Hesse, G. Haerendel, W. Baumjohann, and K. Shiokawa (1999), Flow braking and the substorm current wedge, *J. Geophys. Res.*, *104*(A9), 19895-19903, doi:10.1029/1999ja900173.

Chu, X., R. L. McPherron, T.-S. Hsu, and V. Angelopoulos (2015), Solar cycle dependence of substorm occurrence and duration: implications for onset, *Journal of Geophysical Research: Space Physics*, 2015JA021104, doi:10.1002/2015JA021104.

Chu, X. N., et al. (2014), Development and validation of inversion technique for substorm current wedge using ground magnetic field data, *J. Geophys. Res.*, *119*(3), 1909-1924, doi:Doi 10.1002/2013ja019185.

Dubyagin, S., Sergeev, V., Apatenkov, S., Angelopoulos, V., Nakamura, R., McFadden, J., Larson, D., and Bonnell, J. (2010), Pressure and entropy changes in the flow-braking region during magnetic field dipolarization, J. Geophys. Res., 115, A10225, doi:10.1029/2010JA015625.

Dubyagin, S., V. Sergeev, S. Apatenkov, V. Angelopoulos, A. Runov, R. Nakamura, W. Baumjohann, J. McFadden, and D. Larson (2011), Can flow bursts

penetrate into the inner magnetosphere?, *Geophys. Res. Lett.*, *38*(8), L08102, doi:10.1029/2011gl047016.

Haerendel, G. (1992), Disruption, ballooning or auroral avalanche—On the cause of substorms, paper presented at Proceedings of the International Conference on Substorms (ICS-1), Kiruna, Sweden, 23–27 March 1992, Eur. Space Agency Spec. Publ., ESA SP.

Hones, E. W. (1977), Substorm Processes in Magnetotail - Comments on on Hot Tenuous Plasmas, Fireballs, and Boundary-Layers in Earths Magnetotail, *J. Geophys. Res.*, *82*(35), 5633-5640, doi:Doi 10.1029/Ja082i035p05633.

Hones, E. W., J. R. Asbridge, S. J. Bame, and S. Singer (1973), Substorm Variations of Magnetotail Plasma Sheet from Xsm =-6 Re to Xsm =-60 Re, *Eos T Am Geophys Un*, *54*(1), 58-&.

Keiling, A., et al. (2009), Substorm current wedge driven by plasma flow vortices: THEMIS observations, *J. Geophys. Res.*, *114*(A1), A00C22, doi:10.1029/2009ja014114.

Kepko, L., McPherron, R.L., Amm, O. et al. Substorm Current Wedge Revisited. Space Sci Rev 190, 1–46 (2015). https://doi.org/10.1007/s11214-014-0124-9

Kepko, L. (2018). Magnetospheric constellation: Leveraging space 2.0 for big science. IGARSS 2018-2018 IEEE International Geoscience and Remote Sensing Symposium, IEEE.

Kissinger, J., McPherron, R. L., Hsu, T.-S., and Angelopoulos, V. (2012), Diversion of plasma due to high pressure in the inner magnetosphere during steady magnetospheric convection, J. Geophys. Res., 117, A05206, doi:10.1029/2012JA017579.

Liu, J., V. Angelopoulos, X. Chu, X.-Z. Zhou, and C. Yue (2015), Substorm Current Wedge Composition by Wedgelets, *Geophys. Res. Lett.*, 2015GL063289, doi:10.1002/2015GL063289.

Liu, J., V. Angelopoulos, A. Runov, and X. Z. Zhou (2013a), On the current sheets surrounding dipolarizing flux bundles in the magnetotail: The case for wedgelets, *J. Geophys. Res.*, *118*(5), 2000-2020, doi:10.1002/jgra.50092.

Liu, J., V. Angelopoulos, X. Z. Zhou, and A. Runov (2014), Magnetic flux transport by dipolarizing flux bundles, *J. Geophys. Res.*, *119*(2), 909-926, doi:Doi 10.1002/2013ja019395.

Liu, J., V. Angelopoulos, X. Z. Zhou, A. Runov, and Z. H. Yao (2013b), On the role of pressure and flow perturbations around dipolarizing flux bundles, *J. Geophys. Res.*, *118*(11), 7104-7118, doi:Doi 10.1002/2013ja019256.

McFadden, J. P., C. W. Carlson, D. Larson, M. Ludlam, R. Abiad, B. Elliott, P. Turin, M. Marckwordt, and V. Angelopoulos (2008), The THEMIS ESA

Plasma Instrument and In-flight Calibration, *Space Sci. Rev.*, *141*(1-4), 277-302, doi:10.1007/s11214-008-9440-2.

McPherron, R. L. (1994), The substorm growth phase, *Substorm 2, edited by J.R. Kan, J.D. Craven, and S.-I. Akasofu, Geophysical Institute, University of Alaska, University of Alaska, Fairbanks, AK 99775-0800.*

McPherron, R. L., T. S. Hsu, J. Kissinger, X. Chu, and V. Angelopoulos (2011), Characteristics of plasma flows at the inner edge of the plasma sheet, *J. Geophys. Res.*, *116*, doi:10.1029/2010ja015923.

McPherron, R. L., and X. Chu (2016a), The Mid-Latitude Positive Bay and the MPB Index of Substorm Activity, Space Sci. Rev., 1-32, doi:10.1007/s11214-016-0316-6.

McPherron, R. L., and X. Chu (2016b), Relation of the auroral substorm to the substorm current wedge, Geoscience Letters, 3(1), 1-10, doi:10.1186/s40562-016-0044-5.

McPherron, R. L., and X. N. Chu (2018), The Midlatitude Positive Bay Index and the Statistics of Substorm Occurrence, J. Geophys. Res-Space Phys., 123(4), 2831-2850, doi:10.1002/2017ja024766.

Ohtani, S., H. J. Singer, and T. Mukai (2006), Effects of the fast plasma sheet flow on the geosynchronous magnetic configuration: Geotail and GOES coordinated study, *J. Geophys. Res.*, *111*(A1), A01204, doi:10.1029/2005ja011383.

Pontius, D. H., and R. A. Wolf (1990), Transient Flux Tubes in the Terrestrial Magnetosphere, *Geophys. Res. Lett.*, *17*(1), 49-52, doi:DOI 10.1029/GL017i001p00049.

Runov, A., et al. (2011), Dipolarization fronts in the magnetotail plasma sheet, *Planetary and Space Science*, *59*(7), 517-525, doi:DOI 10.1016/j.pss.2010.06.006.

Runov, A., V. Angelopoulos, M. I. Sitnov, V. A. Sergeev, J. Bonnell, J. P. McFadden, D. Larson, K. H. Glassmeier, and U. Auster (2009), THEMIS observations of an earthward-propagating dipolarization front, *Geophys. Res. Lett.*, *36*, doi:Artn L14106, Doi 10.1029/2009gl038980.

Sergeev, V. (2013), Direct evidence of a two-loop pattern of the substorm current wedge (SCW2L).

Sergeev, V. A., I. A. Chernyaev, V. Angelopoulos, A. V. Runov, and R. Nakamura (2014a), Stopping flow bursts and their role in the generation of the substorm current wedge, *Geophys. Res. Lett.*, *41*(4), 1106-1112, doi:10.1002/2014GL059309.

Sergeev, V. A., A. V. Nikolaev, N. A. Tsyganenko, V. Angelopoulos, A. V. Runov, H. J. Singer, and J. Yang (2014b), Testing a two-loop pattern of the substorm current wedge (SCW2L), *Journal of Geophysical Research: Space Physics*, n/a-n/a, doi:10.1002/2013JA019629.

Shiokawa, K., W. Baumjohann, and G. Haerendel (1997), Braking of high speed flows in the near Earth tail, *Geophys. Res. Lett.*, *24*(10), 1179-1182, doi:10.1029/97gl01062.

Shiokawa, K., et al. (1998a), High-speed ion flow, substorm current wedge, and multiple Pi 2 pulsations, *J. Geophys. Res.*, *103*(A3), 4491-4507, doi:10.1029/97ja01680.

Shiokawa, K., G. Haerendel, and W. Baumjohann (1998b), Azimuthal pressure gradient as driving force of substorm currents, *Geophys. Res. Lett.*, *25*(7), 959-962, doi:10.1029/98gl00540.

Takada, T., R. Nakamura, W. Baumjohann, Y. Asano, M. Volwerk, T. L. Zhang, B. Klecker, H. Rème, E. A. Lucek, and C. Carr (2006), Do BBFs contribute to inner magnetosphere dipolarizations: Concurrent Cluster and Double Star observations, *Geophys. Res. Lett.*, *33*(21), L21109, doi:10.1029/2006gl027440.

Vasyliunas, V. (1970), Mathematical Models of Magnetospheric Convection and its Coupling to the Ionosphere, in *Particles and Fields in the Magnetosphere*, edited by B. M. McCormac, pp. 60-71, Springer Netherlands, doi:10.1007/978-94-010-3284-1_6.

Weygand, J. M., R. L. McPherron, K. Kauristie, H. U. Frey, and T. S. Hsu (2008), Relation of auroral substorm onset to local AL index and dispersionless particle injections, *Journal of Atmospheric and Solar-Terrestrial Physics*, *70*(18), 2336-2345.

Xing, X., L. R. Lyons, V. Angelopoulos, D. Larson, C. Carlson, A. Runov, and U. Auster (2010), Plasma sheet pressure evolution related to substorms, *J. Geophys. Res.*, *115*(A1), A01212, doi:10.1029/2009ja014315.

Xing, X., L. R. Lyons, V. Angelopoulos, D. Larson, J. McFadden, C. Carlson, A. Runov, and U. Auster (2009), Azimuthal plasma pressure gradient in quiet time plasma sheet, *Geophys. Res. Lett.*, *36*(14), L14105, doi:10.1029/2009gl038881.

Xing, X., L. R. Lyons, Y. Nishimura, V. Angelopoulos, E. Donovan, E. Spanswick, J. Liang, D. Larson, C. Carlson, and U. Auster (2011), Near-Earth plasma sheet azimuthal pressure gradient and associated auroral development soon before substorm onset, *J. Geophys. Res.*, *116*, doi:10.1029/2011ja016539.

Yang, J., F. R. Toffoletto, R. A. Wolf, and S. Sazykin (2011), RCM-E simulation of ion acceleration during an idealized plasma sheet bubble injection, *J. Geophys. Res.*, *116*(A5), A05207, doi:10.1029/2010ja016346.

Yao, Z. H., et al. (2012), Mechanism of substorm current wedge formation: THEMIS observations, *Geophys. Res. Lett.*, *39*(13), L13102, doi:10.1029/2012gl052055.

Zhou, X.-Z., V. Angelopoulos, J. Liu, A. Runov, and D.-X. Pan (2014a), Asymmetric braking and dawnward deflection of dipolarization fronts: Effects of ion reflection, *Geophys. Res. Lett.*, n/a-n/a, doi:10.1002/2014GL061794.

Zhou, X. Z., V. Angelopoulos, J. Liu, A. Runov, and S. S. Li (2014b), On the origin of pressure and magnetic perturbations ahead of dipolarization fronts, *J. Geophys. Res.*, *119*(1), 211-220, doi:Doi 10.1002/2013ja019394.